Title
Generation and transport of a low energy intense ion beam

Journal
Journal of Applied Physics, 96(2)

ISSN
00218979

Authors
Bystritskii, Vit.
Garate, E.
Rostoker, N.
et al.

Publication Date
2004

DOI
10.1063/1.1759400

Peer reviewed

Generation and transport of a low energy intense ion beam

Vit. Bystritskii, E. Garate, N. Rostoker, Y. Song, A. VanDrie, M. Anderson, A. Qerushi, S. Dettrick, M. Binderbauer, and J. K. Walters
Tri Alpha Energy Inc., Foothill Ranch, California 92610 and University of California at Irvine, California 92697

V. Matvienko, A. Petrov, A. Shlapakovsky, and N. Polkovnikova
Institute of Nuclear Physics at Tomsk Polytechnic University, Tomsk 634050, Russia

I. Isakov
Institute of High Voltage at Tomsk Polytechnic University, Tomsk 634050, Russia

(Received 3 October 2003; accepted 15 April 2004)

The paper describes experiments on the generation and transport of a low energy (70–120 keV), high intensity (10–30 A/cm^2) microsecond duration H^+ ion beam (IB) in vacuum and plasma. The IB was generated in a magnetically insulated diode (MID) with an applied radial B field and an active hydrogen-puff ion source. The annular IB, with an initial density of $j_i \sim 10-20$ A/cm^2 at the anode surface, was ballistically focused to a current density in the focal plane of 50–80 A/cm^2. The postcathode collimation and transport of the converging IB were provided by the combination of a ''concave'' toroidal magnetic lens followed by a straight transport solenoid section. With optimized MID parameters and magnetic fields in the lens/solenoid system, the overall efficiency of IB transport at the exit of the solenoid 1 m from the anode was ~ 50% with an IB current density of 20 A/cm^2. Two-dimensional computer simulations of post-MID IB transport supported the optimization of system parameters. © *2004 American Institute of Physics.*
[DOI: 10.1063/1.1759400]

I. INTRODUCTION

Magnetically insulated diodes (MID) for generation of high current ion beams (IB) with pulse durations in the range of $10^{-7}-10^{-3}$ s and energy ranges from 10^{-1} to 1 MeV were pioneered by Sudan and Lovelace,[1] Humphries, Sudan, and Wiley[2] at Cornell University, and Morozov and Vinogradova[3] at the Institute of Atomic Energy in Moscow nearly 30 years ago. Due to the large scale research carried out by many leading facilities worldwide,[1–9] MIDs have developed into an advanced and mature technology used for fundamental and applied studies such as inertial fusion, plasma heating, laser pumping, material modifications, neutron flux generation, etc.

Low energy ($10^{-2}-10^{-1}$ MeV), high current density (~10 A/cm^2), microsecond and millisecond IBs are of special interest for such applications as beam propagation across magnetic field to a standoff target and/or beam capture in plasma to maintain field-reversed configurations.[10]

Generation and transport of such a beam still presents a nontrivial problem due to the following:[11]

(a) Incomplete space charge neutralization of the beam by the accompanying electrons during IB transport in the drift space (<0.2%) which results in a residual electric potential in the IB on the order of $2-4V_A(m_e/m_i)$, and subsequently adds to the initial divergence of the IB. An estimate of the average ion transverse velocity ($\beta \sim 5\times10^{-4}$) corresponds to a divergence half angle of one to a few degrees.[12]

(b) Intrinsic ''temperature'' of the IB at the exit from the MID, due to such factors as incomplete IB neutralization, plasma-beam instabilities, azimuthal nonuniformity of plasma density, formation of ''ripples'' at the ion-emitting plasma boundary from the slotted structure of the anode,[13] uncompensated B-field flux behind the plasma-emitting boundary, etc. The dynamics of this boundary depends on the plasma temperature, density, and the mode of MID operation (with and without plasma filling).

(c) A long pulse duration, which precludes the possibility of using smaller AC (anode-cathode) gaps to increase ion current density due to shorting of the gap by the electrode plasma moving inside the gap across the magnetic field with an average velocity of $(2-5)\times10^5$ cm/s.[14] It must be added here that in a MID without a solid anode electrode and with an ion-emitting boundary formed by a magnetic surface, the issue of secondary plasma ceases to be critical, as it was shown by Greenly *et al.* in Ref. 12. The current density limitation could be also overcome by using a MID geometry that provides short ballistic focusing of the IB (e.g., a conical or spherical-shaped anode with focal length of 20–30 cm). The expected degree of IB compression C of the IB using a cone-shaped flat anode can be estimated from the intrinsic divergence γ of the beam and by the relation, $C = 4A_A/\pi(\delta/\cos\theta + 2R\gamma)^2$. Here, A_A stands for the area of the anode annulus, δ is the annulus width, θ is the focusing angle, R is the focal length, and γ is the half angle of intrinsic divergence. For example, with $A = 2.5\times10^2$ cm^2, $\delta = 3.5$ cm, $\theta = 22.5°$, $\gamma = 2°-3°$, and $R = 27$ cm, the compression ratio is between 4 and 6. However, such a dense IB, due to its considerable angle of convergence, cannot be transported large distances. As a result, when propagating freely in vacuum, the IB experiences fast radial expansion and a decrease in density with distance. Various experiments,

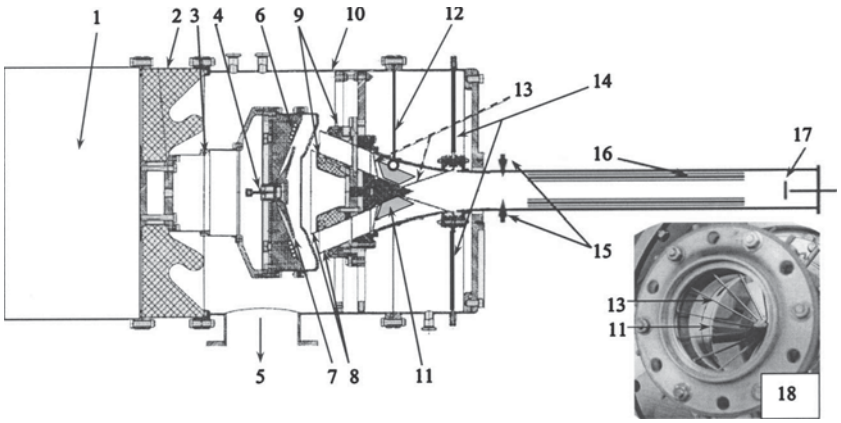

FIG. 1. Schematic of ion beam generator and subsystems. 1, Marx bank; 2, HV insulator; 3, anode stalk; 4, gas puff; 5, to vacuum pump; 6, shock coil; 7, Laval nozzle; 8, cathode blades; 9, B-field coils; 10, vacuum chamber; 11, metal fins, 12, B-dot probe; 13, TML spokes; 14, TML feeds; 15, plasma guns; 16, transport solenoid; 17, multi aperture CFC; 18, Picture of TML (front view).

supported by computer modeling, show that this residual charge imbalance and IB temperature, could result in the virtual disappearance of the beam at distances $\geqslant 1$ m when propagating in vacuum.[15]

Taking these conditions into consideration, a combined ballistic focusing MID with a ''concave'' toroidal magnetic lens (TML) (Ref. 16) and a straight transport solenoid (TS) were implemented in an attempt to substantially increase the density and propagation length of the IB. This work proves that such a combination made possible a significant increase in the transport length of an intense low energy IB.

The paper is organized as follows. Section II of the paper is dedicated to a brief description of the IB generator subsystems. Section III describes the main experimental results on the IB generation and its transport under various conditions. The analysis and discussion are given in Sec. IV. Conclusion, acknowledgments, and references follow.

II. EXPERIMENTAL SETUP

The schematic of the experimental setup is given in Fig. 1. The following is a brief description of the various subsystems.

A. Marx generator

The oil-filled three-stage Marx generator with erected capacitance of 0.27 μF served as the primary source with 1.2–2.5 kJ of stored energy at charging voltages of 30–45 kV. The output Marx current amplitude was in the range of 5–15 kA during the HV (high voltage) phase and 50–60 kA when shorted to the ground via a controlled trigatron-type spark gap. Typical Marx voltage, current, and dynamic impedance wave forms are illustrated in Figs. 2(a)–(c). The impedances in the high voltage and short circuit modes are in the range of 6–20 Ω and 1.8–2 Ω, respectively. The typical voltage overshoot at the front of the pulse was also present in the case with an initial vacuum AC gap.

B. MID

In general, the MID has a conventional annular geometry with focusing AC gap and external radial *B* field which is similar to the MIDs used earlier elsewhere.[4–8,17] However, in difference from these earlier MID systems, where the *B*-field flux separatrix was formed in free space by two sets of *B*-field coils, our design tested in Ref. 17 formed the separatrix at the entrance to the AC gap by the use of a solid conductive anode surface which is nontransparent to the pulsed *B* field. The first use of a conductive slotted anode in a magnetically insulated gap was tested in Ref. 18 by Humphries *et al.* Such an anode design provides a defined position and better stability of the separatrix and conservation of the *B*-field flux in the AC gap during the major portion of the pulse (supporting the closed $E \times B$ drift of the electrons in the AC gap), compared with Refs. 4–8, which is beneficial for the control of MID dynamics.

1. Anode

The anode, with a total area of 250 cm^2, features a brass circular plate with six azimuthal slots providing a geometric transparency of 75%. The AC gap is annular in shape and 8 mm wide. The absence of the external *B* field inside the anode cavity enhanced the efficiency of the hydrogen gas breakdown and formation of plasma. However, it is worth noting that the use of a slotted anode that is nontransparent to a pulsed *B* field may lead to enhanced IB temperature due to sagging of the magnetic flux inside the slots and therefore the formation of a rippled ion-emitting plasma boundary. Special means were used to minimize this effect and are described in the following text.

2. Cathode

The cathode of the MID is formed by two stainless steel coaxial conical blades with an average radius of 20 cm and an apex angle of 45°. The postcathode transport channel is 4.3 cm wide and delivered the converging annular IB to the TML section.

3. Puff valve

The puff valve is conventional in design and was energized by a 100 μF capacitor bank, with an operational voltage between 1.2 and 1.5 kV, a current pulse rise time of 20 μs, and current amplitude of 7–9 kA. The gas flow pressure amplitude, gas rise time and axial thickness for optimal operational parameters (plenum pressures ranged from 0 to 8 mm Hg (gauge), time delay prior to Marx firing was 225–230 μs) were 50 mTorr, 70 μs, and 20–25 mm, respectively.

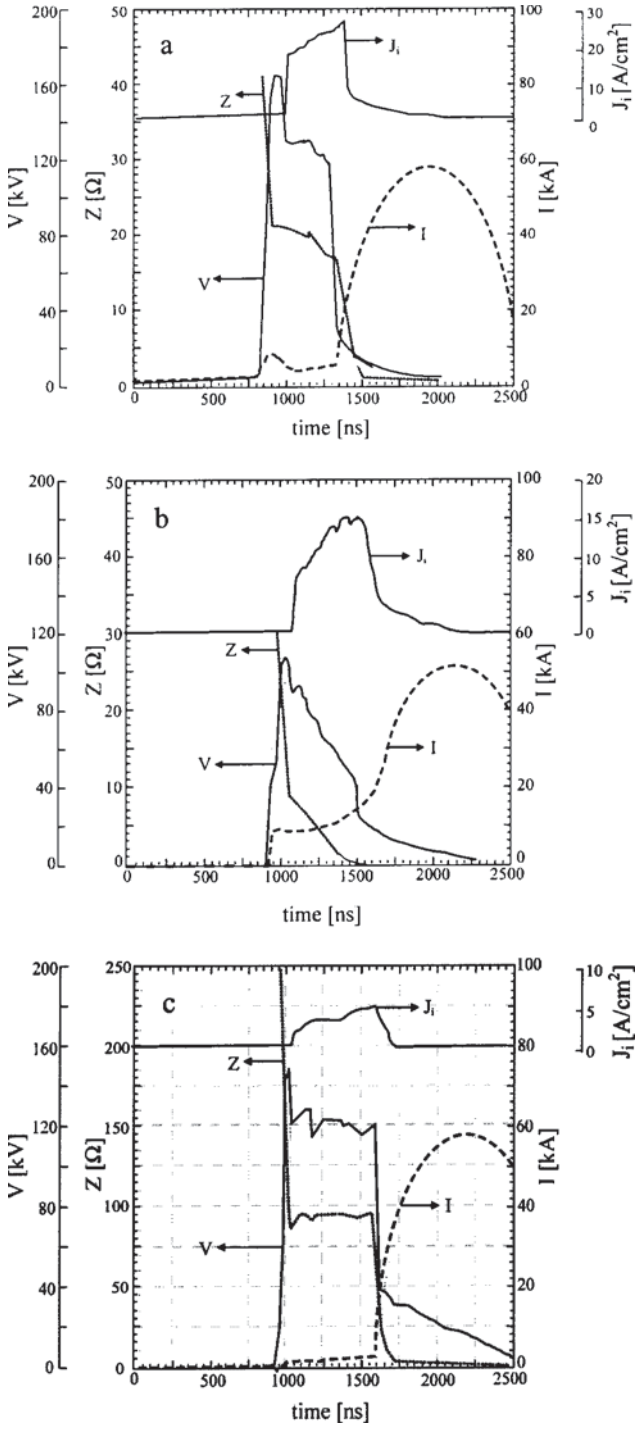

FIG. 2. (a) Typical wave forms for the MID matched-load operation. Z = diode impedance, V = Marx voltage, I = Marx current, J_i = IB current density. (b). Typical wave forms for the MID overloaded operation. (c). Typical wave forms for the MID underloaded operation.

Typical wave forms of the gas pressure as a function of time at various radial distances from the anode surface and puff valve current are given in Figs. 3(a–c).

4. Plasma ion source

The plasma ion source, similar to the type described in Refs. 19 and 20, is located inside the anode cavity and behind the anode plate. The source is fed and triggered via

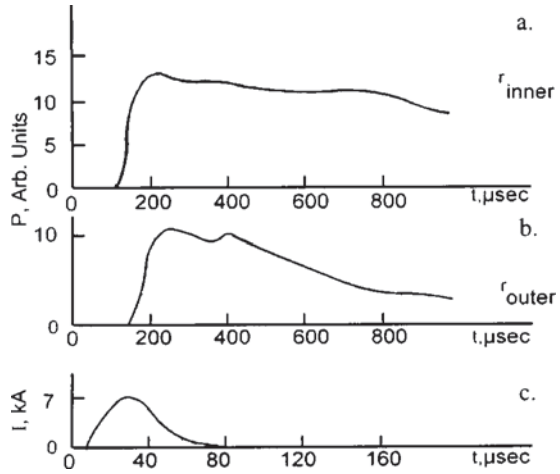

FIG. 3. Typical pressure wave forms of the H_2 gas flow for inner and outer radius of anode, 6 mm from dielectric surface of shock coil assembly. (a) r_{inner} = 9.2 cm (b) r_{outer} = 12.8 cm (c) Puff valve coil current.

decoupling chokes located in the oil volume of the Marx generator. The plasma is generated by a ringing inductive azimuthal breakdown of the radially divergent supersonic H_2 gas flow that is driven by a fast "shock" coil (SC) with a total circuit inductance of 0.5 μH. The plasma produced behind the brass anode is propelled by the Ampere force through the slots into the AC gap where it stagnates along the magnetic surface of the applied radial B field. The schematic of the SC is given in Fig. 4.

Typical current wave forms for optimized gas puff and shock coil parameters are illustrated in Fig. 5. Estimates of the energy delivered to the plasma based on the rate of the current decay and quantity of gas passing through the anode during the SC discharge give values of 20–45 J (i.e., 50–100 and 100–200 eV per molecule) for shock coil charging voltages of 12 and 18 kV, respectively. The plasma density and temperature measured ~3 cm from the dielectric surface, corresponding to the location of the anode slots, was $(2-4)\times10^{13}$ cm^{-3} and ~5 eV with an ion-emission capacity of $\leqslant$20 A/cm^2.

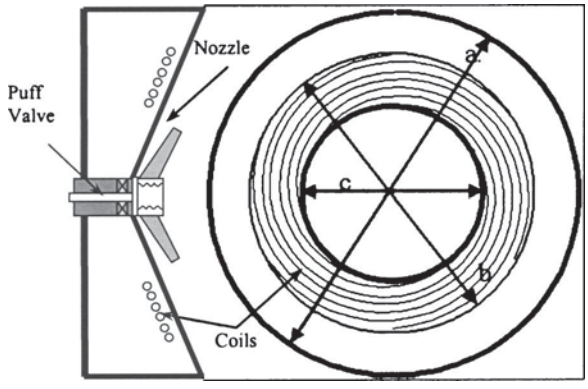

FIG. 4. Sketch of the shock coil windings. Side view (left), Front view (right); (a) 32 cm, (b) 29 cm, (c) 21 cm.

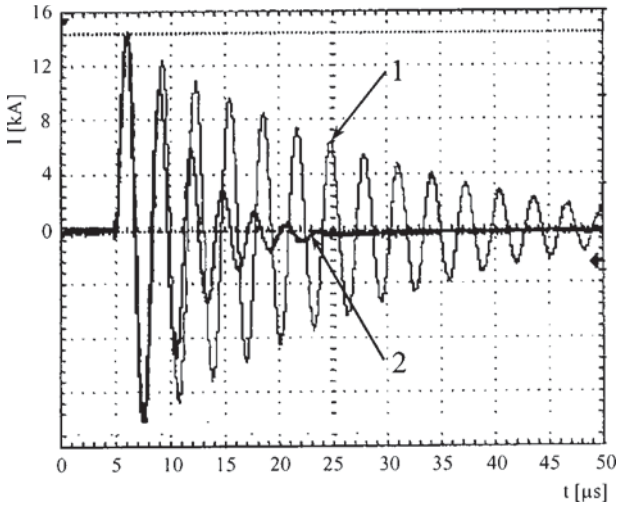

FIG. 5. Typical oscillograms of the shock coil current without (1) and with (2) the breakdown of gas.

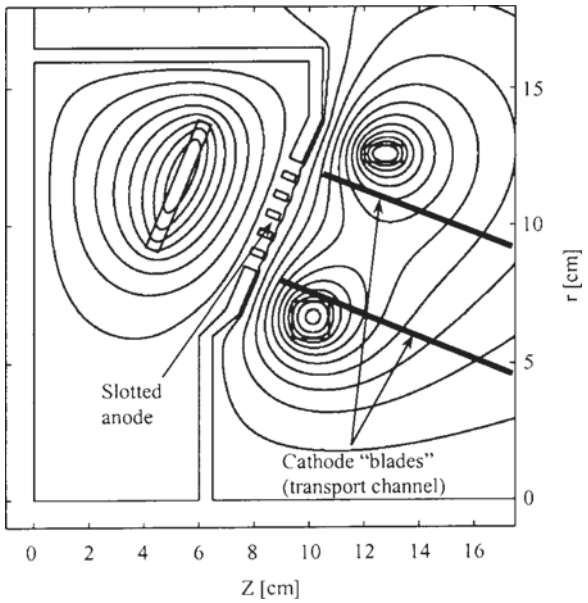

FIG. 6. Magnetic flux lines distribution for the shock coil (left) and diode *B*-field coils (right).

5. AC gap magnetic field

The radial B field in the AC gap and in the postcathode channel was produced as usual[2–9,12] by a pair of ''slow'' coaxial coils positioned near the edge of the cathode ''blades.'' The absence of the external radial B field inside the anode cavity, as mentioned earlier, facilitates plasma formation in the divergent gas flow. The magnetic field we normally operated at was in the range of 2.5–3 kG, which corresponds to $(2-2.5)B_{cr}$. Here, $B_{cr}=1.7(2eV_A/m_ec^2)^{1/2}/d$, where B_{cr} is in kilogauss and d is in centimeters. With a brass anode of $\delta=5$ mm thickness and a skin depth l_s of $\sim 0.1\delta$, where $l_s=c(4\tau_f/\pi\sigma)^{1/2}$, the anode remained practically nontransparent to the insulating pulsed B field. To decrease the sagging of the B-field flux in the anode slots, generation of the plasma, and subsequently the IB, was organized at the maximum of the SC current sine wave when its B-field direction between the slots was in the same direction as that of the MID insulating B field. This occurred on the third half wave of the SC discharge (see Fig. 5). The calculated distribution of the magnetic field lines in the AC gap is given in Fig. 6.

6. Magnetic lens

A magnetic lens with a toroidal B field (TML), featuring a trapezoidal-shape longitudinal cross section formed by 12 radial spokes (optimized to transform the ballistically convergent IB with an average energy of 100 keV and intrinsic divergence of $\gamma=3°$ into a straight one), was installed adjacent to the postcathode convergent coaxial channel. The geometric transparency of the lens was ~95% and ~75% at the peripheral and inner part of the lens, respectively. One-particle ion tracings, with the assumption of full current and space charge neutralization of the IB, were done to optimize the TML configuration and the current amplitude through the lens spokes (20–25 kA). Tracings for three characteristic beamlets (outer, middle, and inner) for a 90 keV IB with 2.5° half angle of divergence through the lens are illustrated in Fig. 7. The energizing of the lens was done by a 120 μF capacitor bank charged to 1.5–2 kV which provided 20–30 kA current pulse through parallel spokes. The maximum length of the lens from the entrance to the exit plane is 150 mm.

7. Transport solenoid

Transport solenoid (TS) consists of a two layer coil wrapped around a dielectric tube 9 cm in diameter and 60 cm in length. The TS entrance is located 11 cm from the exit of the TML. The solenoid was energized by a 160 μF capacitor bank charged to 1.4–2.3 kV with a characteristic impedance of 0.8 Ω. The TS system is able to provide a pulsed magnetic field in the range of 4–7 kG with a rise time of 200 μs. The expected optimal B field for a given length L of the solenoid (determined by a one-particle approximation and based on the condition of the IB making one full turn in the solenoid during its flight) can be estimated from the expression $B=2\times10^7\beta/L$, which for this experiment gives $\beta=1.5\times10^{-2}$, $L=60$ cm, and $B=6$ kG. Because of the substantial energy spread in the ''real'' IB during the pulse and its initial

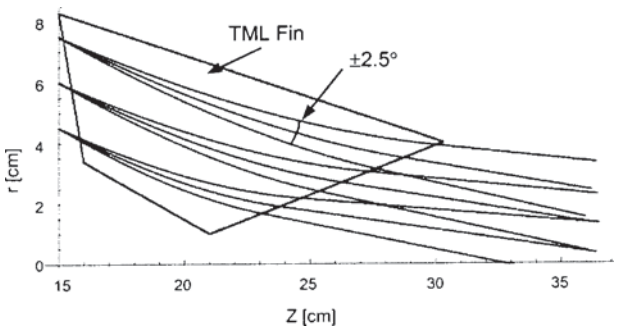

FIG. 7. Calculated trajectories for three characteristic beamlets through the TML. Half angle of divergence is $\pm2.5°$, $I_{\text{lens}}=23$ kA, $E_i=90$ keV. Here, Z is the distance from the anode.

divergence ($\gamma \sim 3°$) the optimal value selected experimentally was slightly different from the estimates given by idealized calculations.

8. Plasma guns

To enhance the degree of neutralization in the IB two cable-type plasma guns were inserted into the intermediate section between the end of the TML and the entrance to the TS. The plasma guns were energized by a 0.05 μF capacitor bank charged to 10–15 kV. The microwave density measurements of the plasma produced by these guns demonstrated cutoff at the frequency of 40 GHz, which corresponds to a plasma density $>10^{13}$ cm^{-3}.

III. EXPERIMENTAL RESULTS

A. Diagnostics

The main parameters of the subsystems (voltages, current amplitudes, and other pulse wave forms) were measured by active voltage dividers, *B*-dot probes, and self-integrating Pearson (Rogowsky) coils. The current density of the IB at various distances from the anode in various conditions (e.g., in vacuum or ambient plasma with and without transverse magnetic field) was measured by a system of collimated Faraday cups (CFC) with an applied bias voltage (-30 to -100 V) and/or transverse magnetic field (400–600 G). The integrated-in-time energy stored in the IB at various distances from the anode for different conditions was measured by a calorimeter. The ambient plasma density and its temperature were measured by double and triple Langmuir probes[21] and by microwave cutoff at 40 GHz.

B. Time sequence of subsystems operation

Triggering of all subsystems was done via computer from a master trigger. The spark gaps of the Marx generator, shock coil, plasma guns, and crowbar were triggered by HV pulses of 16–20 kV amplitude generated by independent pulsers. All other subsystems (MID *B* field, TML, puff valve, and TS) were energized by ignitrons. The chain of events, including appropriate time scales, is illustrated in Fig. 8. The average jitter between triggering the Marx, crowbar, and shock coil was <50 ns. For all ''long'' pulse subsystems of multimicrosecond scale, the jitter was <0.1 μs.

C. IB ballistic focusing

Typical MID operation, with an AC gap of 8.0 mm and $B=2.5-3.0$ kG, produced an average current density of the IB, j_i, near the exit of the AC gap of 6–12 A/cm^2 and 10–20 A/cm^2 for V_A in the range of 70–100 kV, respectively (matched mode). These values are estimated to be $(2-3)j_{CL}$. With an active anode area of 250 cm^2 these current densities give an IB current amplitude of 2–3 kA and a total average MID current of 4–6 kA. These results correspond to ~50–70 % IB generation efficiency in the diode. In a typical pulse, the MID current wave form has a short duration spike of a few tens of nanoseconds, due to the fast erosion of the low density plasma already present in the AC gap, and the voltage pulse front had an overshooting spike typical for a plasma erosion switch operation.[22] The voltage

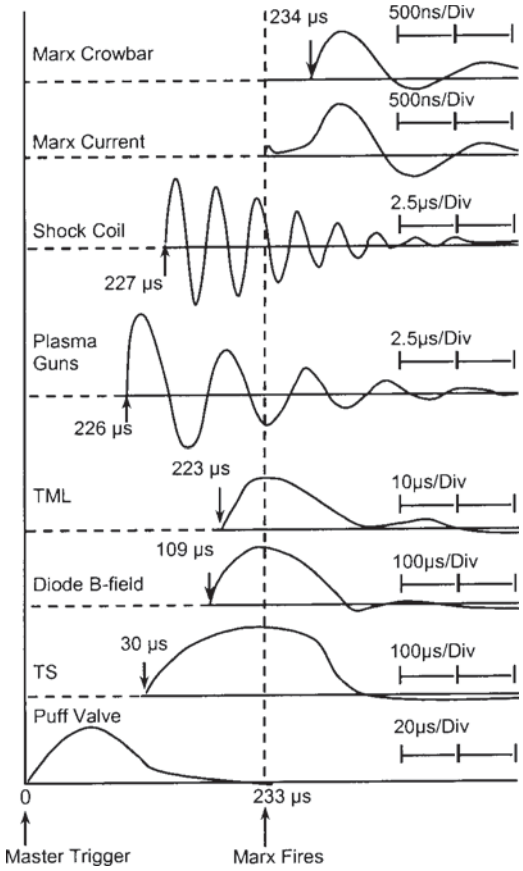

FIG. 8. Typical oscillograms for generator subsystems and respective time sequence.

spike was followed by a fairly constant voltage plateau and a slow current rise which corresponds to a matched-load operation with a ''slow'' change of the AC gap due to the plasma motion across magnetic field. The speed of the plasma motion was estimated to be $(0.2-0.5)\times 10^6$ cm/s with a *B* field of $(2-3)B_{cr}$ based on the pulse duration up to the shorting when operating without the crowbar.

In the case of an underloaded MID (B field$>3B_{cr}$), the voltage overshoot was significant (up to $1.5V_{\mathrm{Marx}}$) and was accompanied by a low current amplitude and a premature crowbar self-breakdown.

By changing the MID parameters, we could operate with a plasma prefilled AC gap (overloaded mode) resulting in higher IB current densities and lower IB energies. In this mode of operation, with relatively high IB current densities ($j_i \sim 20$ A/cm^2), but significantly larger MID current amplitudes ($I \sim 10-15$ kA) and lower MID voltages ($V_A \sim 60-70$ kV), the IB generation efficiency dropped to ~30%. Typical pulses for the three modes of MID operation are presented in Figs. 2(a–c).

The ballistic conical focusing of the IB produced a current density (measured by two CFC with transverse *B* field and low amplitude negative bias) in the range of 50–80 A/cm^2 at the central part of the focal plane 27 cm from the anode. The autographs of the IB in the focal region, obtained with the thermosensitive paper, were ~7 cm in diameter. This result corresponds to an IB divergence half angle of $<3°$. Based on this data, the total IB amplitude in the focal

plane was estimated to be between 1.3 to 1.8 kA. Autographs of the IB from heat sensitive paper at a distance of 30–35 cm from the anode featured a cross section of tubular shape. Also, it was found that irregular shaped autographs of the IB correlated to ''bad'' shots with high electron losses. To decrease the divergence of the IB during its propagation inside the converging annular channel, the bare metal walls were lined with a dielectric film. The dielectric film served as a plasma source due to its bombardment by the peripheral flow of ions and related surface breakdown. The autographs of the IB produced on heat sensitive paper placed along the channel wall were most pronounced near the inner wall at the entrance from the AC gap to the channel. The overall transport efficiency of the IB through the channel was estimated to be ~60%. This estimate includes the postcathode space geometric transparency of ~90%.

D. TML operation

Several modifications of the TML were tested for their collimating performance. Experiments revealed that the vacuum TML does not provide an efficient space charge neutralization of the IB resulting in gross ion losses to the TML walls. In the first modification, two cable plasma guns, fabricated of HV coaxial cable, were positioned opposite to each other in the middle of the TML and flush with its outer wall. The cable guns were fired before ion beam generation to provide sufficient plasma prefilling. The optimal time delay between their firing and the triggering of the Marx was in the range of 5–6 μs. At longer time delays, the plasma prefilling overloaded the MID. In the second configuration, five cable plasma guns were located 17 cm downstream from the TML exit and fired axially toward the TML. This configuration proved to be more beneficial for IB transport through the drift tube than through the TML. In the third modification, four trapezoidal-shape radial fins covering >90% of the longitudinal cross section of the TML were attached to the inner cone of the lens and positioned so that the fins intersected the toroidal magnetic field lines at 90°. This design proved to be the best regime for IB transport through the TML and worked as follows: secondary electrons, generated at the surface of the fins due to ion bombardment, traveled along the TML *B*-field lines and provided fast neutralization of the polarization *E* field in the IB. As a side note, adding plasma prefilling did not improve the performance of the TML with radial fins. Experimental data showed that the optimal range for the TML current was 26–30 kA. The scaling of the IB density at the TML exit as a function of TML current was illustrated in Fig. 9. Adding the finite solid angle of the fins to the 0.92 geometric transparency of the lens results in a total TML transparency of ~85%.

E. Transport solenoid

Application of the TS after the TML makes it possible to separate the exit of the IB accelerator from the target by a significant distance (>1 m). The ions entering the solenoid with a small transverse velocity meet B_r-field and follow a spiral trajectory, with a guiding center shifted off-axis at $\sim 0.5R_{\mathrm{ent}} = R_{\mathrm{Larmor}}$ (here R_{ent} is the radial coordinate of the ion at the entrance and R_{Larmor} is the ion Larmor radius). The respective envelope of the IB is shaped like a spindle. To minimize the residual rotational energy of the ions at the exit from the solenoid, the net magnetic flux crossed by the ion must be small and can be obtained if the ions perform an integer number of full rotations when traveling through solenoid (i.e., if the radial coordinate at the entrance to the solenoid is equal to its radial coordinate at the exit). The appropriate solenoid length can be estimated by the formulas (without the consideration of edge error fields)

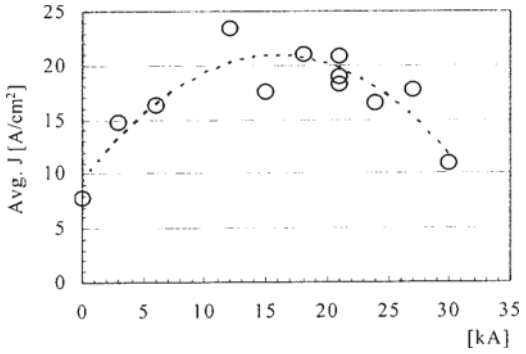

FIG. 9. Averaged IB cross sectional current density vs TML current. Measured by CFC array, $Z = 8$ cm from TML exit, IB energy −90 keV.

$$L_{\mathrm{sol}} = 2\pi N(3.1\times 10^6)/B[V_o^2 \cos^2\theta - V_\perp^2]^{1/2},$$

where

$$V_\perp = eBR_s/2m_p c.$$

Here, $N = 1,2,...$ is the integer number of ion rotations, V_0 is the initial velocity of the IB, $\cos\theta$ is the intrinsic divergence of the ion beam, $V_\perp$ is the rotational velocity acquired when entering the solenoid, R_s is the radius of solenoid clearance, and B is the solenoid B field. For example, with an IB average energy of 100 keV, an initial half angle of divergence of 2.5°, a TS length of 60 cm and the TS entrance located 13.5 cm from the TML exit, the optimal magnetic field is ~ 6.3 kG.

One-particle trajectory calculations of the ions moving through the TML-TS system were done for several characteristic beamlets with a given angular spread under the assumption of full space charge and current neutralization. The optimization of lens-solenoid system was done to minimize the exit transverse velocity of the IB. Typical tracings of the central and peripheral ion beamlets are given in Fig. 10 and Table I presents their entrance and exit data.

Experiments on scaling the efficiency of IB transport as a function of solenoid B field with a given current through the TML provided an optimal combination of $I_{\mathrm{lens}} \sim 20$ kA and a TS magnetic field of ~7 kG. Figure 11 illustrates the measured average IB density in a 3 cm diameter paraxial region within and outside the solenoid. Due to the initial angular divergence of the IB, losses to the walls took place in the first 20 cm of the TS.

The average distance between the maximums in the curve was ~36 cm and correspond to a rotating IB with an

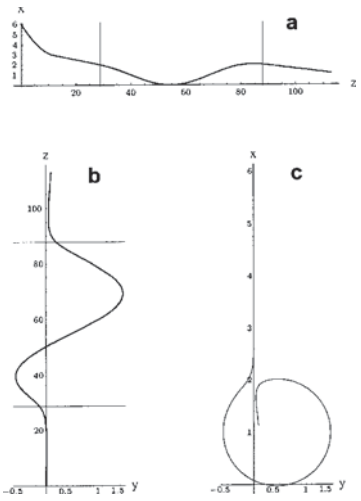

FIG. 10. Traced ion trajectory (one middle beamlet) through the combined TML and TS system 8 for a 90 keV IB. (a) *x-z* plane, (b) *y-z* plane, and (c) *x-y* plane. All dimensions are in centimeter. The straight lines in (a) and (b) indicate length of solenoid.

average energy of 90 keV. The finite angular and energy spread of the IB smooth the oscillations of the measured density.

The average efficiency of IB transport through the solenoid was >90%. However, after leaving the solenoid, the density of the IB dropped from 15–20 to 3–4 A/cm^2 at a distance of 30 cm from the TS exit.

IV. DISCUSSION

As shown by the experiments, effective control of the microsecond MID impedance and IB parameters could be obtained when operating with conserved *B* flux in the AC gap. At the same time the IB divergence at the AC exit of $\gamma \sim 3°$ corresponds to a transverse ion energy of ~200 eV. As mentioned earlier, this could be ascribed to several factors such as (1) incomplete IB neutralization, (2) instabilities of the plasma boundary when it stagnates against the radial B_r field, (3) azimuthal nonuniformity of the plasma boundary density, (4) ripples in the ion-emitting boundary pertinent to the slot structure of the anode, and (5) residual *B* flux left behind the plasma-emitting boundary. Factor (1) is inherent in the peripheral layers of the IB generated in the MID and could be mitigated by providing a convex shape of the equipotential *B* field surfaces in the AC gap,[3] for example, by using a spherical-shaped solid anode. The importance of factor (2) evidently decreases with an increase of the *B*-field strength near the anode surface and its rate of rise, thus working with a faster pulsed *B* field could be beneficial, to some limit. Factor (3) seems to be responsible for the correlation between the irregular structure of the IB autographs and the occasional bad shot with high electron losses and depends on the mechanical performance of the puff valve. Factor (4) pertains to the phenomenon of equipotentialization[3] of the *B* surfaces in the AC gap and *B*-field sagging in the anode slots. We estimated the position and sinuosity of the emitting plasma surface at the moment of the HV pulse arrival (based on its average velocity across the *B* field in the AC gap $\sim 5\times10^5$ cm/s) (Ref. 14) to be 3 mm and ~2°. This corresponds to a final average divergence angle of ~1° after crossing the accelerating gap. The ion transverse velocity acquired due to the residual B_r magnetic flux left behind the ion-emitting boundary [factor (5)] in the plasma and diffused through the anode can be estimated using the expression $\beta_{\text{trans}} = B\ (\text{kG})\ \delta/(3\times10^3)$. For our experimental parameters, this corresponds to an IB divergence of ~0.2–0.3°. The remaining causes for the divergence of the IB increasing to ~2° are most likely due to the first two factors.

The effect of the slots could be mitigated by the use of an additional thin anode transparent to the *B* field with a set of ''fine'' slits or holes. Such a foil located a few millimeters in front of the thick brass anode, where the ''ripples'' are much smaller, would define a more smooth emitting plasma boundary and provide a ''colder'' IB. The use of an additional compensating *B*-field flux to form a smooth plasma emitting surface, as exploited in Ref. 12, instead of a solid metal anode could present a trade-off between the required reproducibility and temperature of IB.

The IB in our experiments is almost fully neutralized (≥99.8%) when traveling inside the TML and TS. Mainly, the intrinsic temperature of the IB limits the overall transpar-

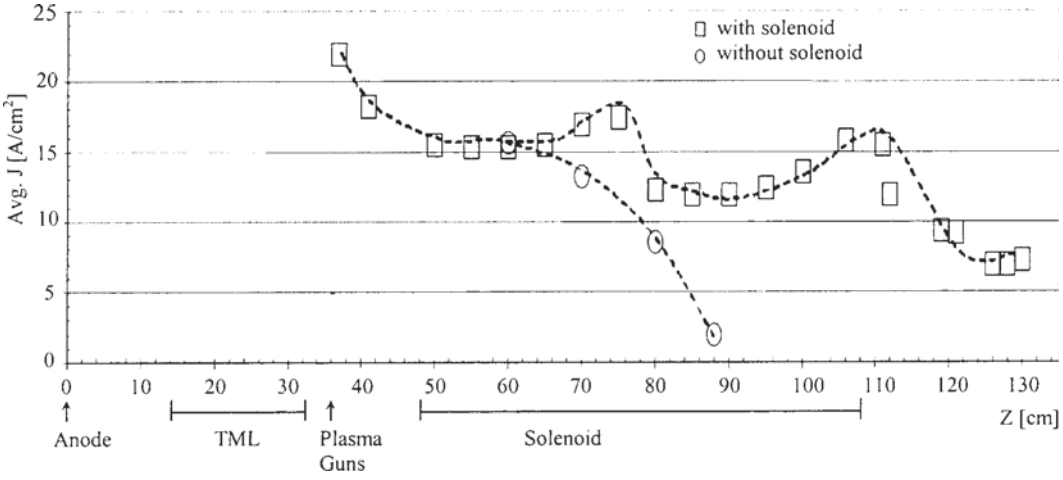

FIG. 11. Average IB current density in the paraxial region (measured by CFC array) vs propagation distance from anode. IB energy −90 keV.

ency of the TML due to the lateral losses of the ions on the metal fins and channel walls. Optimization of the TML by varying its driving current is possible over a wide range, but the efficiency depends on the energy spread of the IB. The limitation imposed on the spread of the IB energy could be mitigated by using a pulse forming element instead of an *RC* discharge and a smaller ballistic angle with lower TML *B* field. Transition from conical to spherical focusing may also improve the TML operation.

When leaving the TML, the IB transits to a space free of toroidal *B* field where the buildup of electrons on the closed *B*-field lines take place resulting in a local charge imbalance and the appearance of axial and radial *E* fields. This results in a slowing down and fast divergence of the IB upon exiting the TML.[23] The addition of plasma in this region appears to improve the situation. When propagating inside the TS, the initial divergence of the IB seems to be the main contributor to beam loss on the solenoid walls. This imposes a limit on the minimum diameter of the TS, D_{TS}. In the case of an H^+ beam, D_{TS} can be estimated as

$$D_{\mathrm{TS}} \geqslant 2[D_{\mathrm{IB}} + (3\times 10^3)\beta\gamma B^{-1}],$$

Here D_{IB} is the diameter of the IB at the exit from the TML, *B* is in kilogauss, β is the ratio v/c, γ is in radians and is the IB divergence half angle at the TS entrance. Based on the measured $\gamma \sim 3°$, a D_{IB} of 8 cm and a *B* field of 5–7 kG, the estimated D_{TS} should be >9 or 9.6 cm, respectively. Our D_{TS} was limited due to the injection port size and was therefore 10% smaller than the above estimate.

At the exit from the TS to free space (similar to the situation at the TML exit) the IB again acquires a space charge imbalance because the free axial motion of the neutralizing electrons with the IB becomes impaired. Here the accompanying electrons are confined to move along the radially expanding magnetic lines. Again, this results in the buildup of *E* field with radial and axial components and a respective drag on the IB in the $E\times B$ environment.

Indicated by the experiments, the IB with an initial divergence angle of $\gamma \sim 3°$ and density of 15 A/cm^2 drops five to ten times in density and has a final divergence angle of 14–15° at a distance of 30 cm from the TS exit. It is worth noting that in contrast to the situation at the TML exit, the addition of plasma with a density of $\sim 10^{13}$ cm^{-3} did not significantly decrease the IB divergence in free space, which indicates the persistence of an *E*-field normal to magnetic lines in the plasma. The absence of a nearby conducting surface makes it impossible for the fast neutralization of the *E* field on the time scale of the IB pulse duration. The use of a metal screen crossing the *B*-field lines in the vicinity of the TS exit may be beneficial for IB transport.[24]

V. CONCLUSIONS

Experiments were carried out on the formation and propagation of a low energy (70–120 keV), high density (10–30 A/cm^2) microsecond duration IB. Efficiencies up to 50% and 70%, respectively, were obtained for generation and transport to distances >1 m using a novel system that combined a large area MID with ballistic focusing, a TML and a TS. Operation of the MID with a solid anode provided effective control of electron losses during the main portion of the pulse, thereby, causing a smaller energy spread of the IB. At the same time, the use of a slotted brass anode surface together with residual space charge of the IB and other causes (instabilities, occasional plasma azimuthal nonuniformity) resulted in IB "warming" ($\geqslant$200 eV). Postsolenoid propagation of the IB is further impaired by a space charge imbalance buildup at the transition from TS to free space. Additional means for "cooling" the IB in the AC gap, such as a thin foil anode in front of the solid one and grounded metal screens placed near the exit from the TS, may be useful for long distance transport needed in various applications (inertial confinement fusion, plasma heating, field reverse configuration, etc.).

ACKNOWLEDGMENTS

The authors would like to thank Professor H. Monkhorst, Dr. F. Wessel, and Dr. W. Heidbrink for stimulating discussions and N. Debolt, M. Morehouse, S. Armstrong, and G. Strashnoy for their technical support during the experiment. This work was supported by UCI and Tri Alpha Energy, Inc.

[1] R. N. Sudan and R. V. Lovelace, Phys. Rev. Lett. **31**, 1174 (1973).
[2] S. Humphries, R. N. Sudan, and L. Wiley, J. Appl. Phys. **47**, 2382 (1976).
[3] A. I. Morozov and A. K. Vinogradova, *The Physics and Application of Plasma Accelerators*, (Nauka Minsk, 1974), in Russian.
[4] W. A. Noonan, S. C. Glidden, J. B. Greenly, and D. A. Hammer, Rev. Sci. Instrum. **66**, 3448 (1995).
[5] H. A. Davis *et al.*, J. Appl. Phys. **82**, 3223 (1997).
[6] G. Yonas, in Proceedings of the 12th International Conference on High Power Particle Beams, Haifa, Israel, 1998, edited by M. Markovits and J. Shilkoh, Vol. 1, p. 165.
[7] Physics of Intense Light Ion Beams, edited by H. J. Bluhm (Forschungszentrum, Karlsruhe, 1999).
[8] X. P. Zhu, M. K. Lei, Z. H. Dong, and T. C. Ma, Rev. Sci. Instrum. **74**, 47 (2002).
[9] K. Masugata, Y. Kawahara, Y. Maetsubo, Y. Doi, K. Iwao, T. Takahashi, Y. Tanaka, H. Tanoue, and K. Arai, in Proceedings of the 13th International Pulsed Power Conference, Las Vegas 2001, edited by R. Reinovsky and M. Newton, Vol. 2, p. 1366.
[10] M. W. Binderbauer and N. Rostoker, J. Plasma Phys. **56**, 451 (1996).
[11] V. M. Bystritskii and A. N. Didenko, *High Power Ion Beams* (AIP, New York, 1990).
[12] J. B. Greenly, M. Ueda, G. D. Rondeau, and D. A. Hammer, J. Appl. Phys. **63**, 1872 (1987).
[13] V. Fedorov, in Proceedings of the 10th International Conference on High Power Particle Beams, San Diego, CA, 1994 edited by G. Cooperstein, Vol. 1, p. 45.
[14] I. Gleizer, A. Didenko, Yu. Usov, V. Tsvetkov, and A. Shatanov, Zhurnal Techn. Physik **50**, 1323 (1980).
[15] V. M. Bystritskii *et al.* Sov. J. Plasma Phys. **14**, 262 (1988).
[16] A. Mohri, K. Ikuta, and J. Fuijita, Jpn. J. Appl. Phys. **20**, 1148 (1977).
[17] A. Petrov, N. Polkovnikova, V. Tomacheva, V. Matvienko, and A. Shlapakovsky, *Book of Abstract International Conference on Materials Modification with Particle Beams and Plasma Flows* (Tomsk, Russia, 2002), Vol. 1, p. 8.
[18] S. Humphries, Jr. *et al.*, J. Appl. Phys. **51**, 1876 (1980).
[19] C. L. Dailey, H. A. Davis, and B. R. Hayworth, Report No. AFPL-TR-73-81, 1973 (unpublished).
[20] S. Humphries, Jr., R. J. M. Anderson, J. R. Freeman, and J. Greenly, Rev. Sci. Instrum. **52**, 162 (1981).
[21] H. Ji *et al.*, Rev. Sci. Instrum. **62**, 2326 (1991).
[22] P. S. Anan'in *et al.*, Sov. J. Plasma Phys. **17**, 69 (1991).
[23] F. J. Wessel, N. Rostoker, A. Fisher, H. Rahman, and J. H. Song, Phys. Fluids B **2**, 1467 (1990).
[24] D. A. Baker and J. E. Hammel, Phys. Fluids **8**, 713 (1965).